Optics Letters

An oscillator-driven, time-resolved optical pump/NIR supercontinuum probe spectrometer

Manita Rai,[1,†] Wesley E. Deeg,[1,†] Baozhu Lu,[1] Katrina Brandmier,[2] Ashtyn M. Miller,[1] and Darius H. Torchinsky[1,*]

[1]Department of Physics, Temple University, Philadelphia, Pennsylvania 19122, USA
[2]Department of Chemistry, DeSales University, Center Valley, Pennsylvania 18034, USA
*Corresponding author: dtorchin@temple.edu
†These authors contributed equally to this work.

Received 25 October 2022; revised 9 December 2022; accepted 16 December 2022; posted 21 December 2022; published 17 January 2023

We present a novel, to the best of knowledge, time-resolved, optical pump/NIR supercontinuum probe spectrometer suitable for oscillators. A NIR supercontinuum probe spectrum (850–1250 nm) is generated in a photonic crystal fiber, dispersed across a digital micromirror device (DMD), and then raster scanned into a single element detector at a 5 Hz rate. Dual modulation of pump and probe beams at disparate frequencies permits simultaneous measurement of both the bare reflectance R and its photoinduced change ΔR through lock-in detection, allowing for continuously self-normalized measurement of $\Delta R/R$. Example data are presented on a germanium wafer sample that demonstrate for signals of order $\Delta R/R \sim 10^{-3}$, a 2.87 nm spectral resolution and $\lesssim$ 400 fs temporal resolution pre-recompression, and comparable sensitivity to standard time-resolved, amplifier-based pump–probe techniques.

https://doi.org/10.1364/OL.479061

Ultrafast pump–probe spectroscopy is an effective tool for studying a wide array of physical processes, ranging from photoexcited carrier dynamics to collective modes of symmetry breaking states, to the chemistry associated with photodissociation and photosynthesis [1–14]. However, the need for electronic resonance may restrict observation of some of these effects to select ranges of incoming photon energy, meaning that proper data interpretation can require measuring material responses over a broad range of wavelengths. To this end, optical pump supercontinuum probe spectroscopy was developed and implemented to study the real time evolution of a photoexcited system as a function of photon energy [15].

In a conventional optical pump–supercontinuum probe measurement, the broadband probe is generated through filamentation in a nonlinear solid or liquid medium [16–19]. After being reflected by the sample, the probe is then dispersed across a CCD camera and analyzed by averaging the output over several pulses, normalizing against a reference to record the time-resolved change in reflectivity or absorbance. While the parallelized detection afforded by a camera allows for relatively quick data acquisition, there are limiting disadvantages to this approach. Supercontinuum generation in bulk media requires high laser fluences, restricting experimental apparatuses to amplified laser systems. This, in turn, leads to lower repetition rate experiments at higher excitation fluences that may damage a sample or disrupt an electronically ordered state. The use of a CCD camera also precludes denoising through lock-in detection and often limits experiments to the visible spectrum, requiring NIR CCD technology to access lower energy processes.

In this Letter, we demonstrate a novel technique based on single-pixel imaging [20,21] to measure photoinduced changes in reflectivity over a broad spectral range. This apparatus is designed around a nonlinear photonic crystal fiber (PCF) that can generate a broad supercontinuum spanning the wavelength range ~ 400–1600 nm using ~ 1 nJ scale energy pulses from a femtosecond oscillator [22,23]. Narrow subbands of the dispersed spectrum are then reflected into a single-element detector by a digital micromirror device (DMD) and measured every 500 μs by MHz-frequency lock-in detection before the next wavelength band is measured. Rapid cycling through the entire spectrum at 5 Hz allows for additional denoising of the data through signal averaging. Below, we provide a detailed description of this apparatus, its calibration, and an example application to a (110) germanium wafer test sample.

Figure 1 shows a layout of the experimental setup, while a full catalog of the important part numbers, as well as experimental parameters, can be found in Supplement 1. The source was a Ti:Sapphire laser (Coherent, Vitara-T-HP) lasing at 800 nm at a repetition rate of 80 MHz with a pulse duration of 25 fs and a usable output power of ~ 600 mW (~ 200 mW was reserved for pumping a regenerative amplifier not used here). A chirped mirror pair (CM; Thorlabs, DCMP175) compensated for the dispersion common to pump and probe beams before supercontinuum generation. The beam was then split using a beam splitter and both pump and probe beams chopped using two acousto-optic modulators (Isomet, M1142-SF80L-0.5) that were driven synchronously with each other but asynchronously with the laser. The probe was chopped as a 50% duty-cycle square wave at $f_1 = 3$ MHz using a reference signal provided by a function generator (RIGOL, DG1022Z) to preserve pulse-to-pulse stability of the generated supercontinuum, while the pump was chopped as a sine wave at $f_2 = 4.3$ MHz using the auxiliary output of a lock-in amplifier (Zurich Instruments, MFLI)

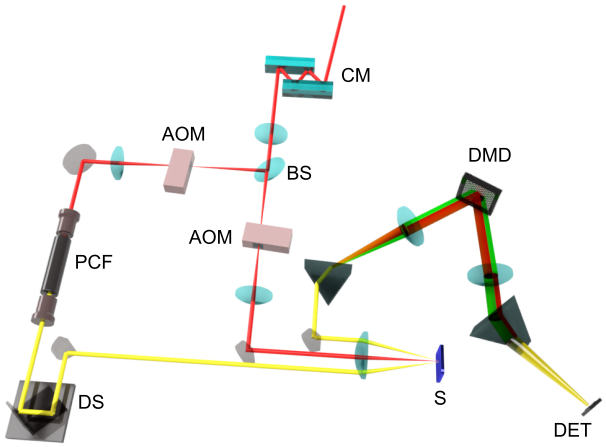

Fig. 1. Layout of spectrometer. CM, chirped mirrors; BS, beam splitter; AOM, acousto-optic modulator; PCF, photonic crystal fiber; DS, delay stage; S, sample; DMD, digital micromirror device; DET, single-element detector.

synchronized to the function generator through their 10-MHz clocks. Dual modulation permitted ΔR to be recovered free of pump-scatter artifacts at the difference frequency $f_2 - f_1 = 1.3$ MHz while also allowing for R to be measured simultaneously by recording the signal at f_1. The normalization $\Delta R(t)/R$ was performed in software after data acquisition was complete.

The chopped pump beam was focused onto the sample with a reflective objective (RO; Edmund Optics, 68-188) to provide photoexcitation. The modulated probe beam was coupled into a nonlinear photonic crystal fiber (NKT Photonics, Femtowhite 800) with ~ 38% coupling efficiency using a 20× objective lens (Newport, M20X), resulting in 31 mW of emitted supercontinuum. We note that this is half the overall probe power due to the 50% duty cycle due to chopping. The supercontinuum output was recollimated by a 40× objective lens (Newport, M40X), mechanically delayed by a motorized linear stage, and then overlapped with the pump beam on the sample by focusing through the RO. After being reflected by the sample, the probe beam was recollimated by the RO, dispersed through a prism (Eksma optics, 320-8525), recollimated by an achromatic lens (Thorlabs, AC508-150-B), and then incident onto the DMD (Texas Instruments, DLP Lightcrafter 6500 EVM).

We programmed the DMD "patterns," defined as matrices the size of the DMD micromirror array (1920 × 1080 pixel), to reflect only a small subset of the spectrum into the detector at a time by setting five columns of pixels to the "ON" state while the rest of the elements were set to the "OFF" state; the OFF-state component of the spectrum was rejected into a beam block. The DMD was triggered to step from pattern to pattern by the function generator via a 2-kHz clock signal, thus raster scanning through the spectrum with an exposure time of 500 μs per data point. Each pattern was chosen so that the five "ON" pixels did not overlap with those of the preceding or subsequent patterns.

The probe beam reflected by the DMD was collected by a lens (Thorlabs, AC508-150-B), passed through a second prism, and focused into an amplified InGaAs detector (Thorlabs, PDA20C2) that was input into a lock-in amplifier with both high-frequency (MF-F5M) and multi-demodulator (MF-MOD) options. The probe frequency f_1 and difference frequency $f_2 - f_1$ were both measured using a 25 μs lock-in time constant and a 32 dB/oct filter slope. The demodulated output from the lock-in was measured through the device's auxiliary outputs by a data acquisition card (National Instruments, PCI 6143) that sampled the demodulated data from both channels simultaneously as triggered by a counter card (National Instruments, PCI 6601) synchronized to the setup through the 2 kHz output of the function generator and timed to record the signal after 19 time constants had elapsed since the pattern had been switched.

Although the fiber produced strong output in the 450–750-nm range, supercontinuum generation in its anomalous dispersion regime (i.e., <750 nm and >1250 nm) generates mutually phase coherent solitons that produce artifacts in the data that cannot be removed in post-processing. The unsuitability of this output for this application is consistent with other reported spectroscopic applications of supercontinua generated in nonlinear PCFs [24]. Hence, we have chosen to work in the normal dispersion regime of the fiber, spanning 750–1250 nm.

To calibrate the setup, we measured R using bandpass filters at the following wavelengths: 760 nm (Thorlabs, FB760-10), 810 nm (Thorlabs, FB810-10), 830 nm (FB830-10), 900 nm (FB900-10), 950 nm (FB950-10), 1000 nm (FB1000-10), 1050 nm (FB1050-10), 1100 nm (FB1100-10), 1150 nm (FB1150-10), and 1200 nm (FB1200-10). Data obtained with a specific bandpass filter were modeled by a Gaussian equation to match the manufacturer-specified Gaussian line shape of the passband and fit to determine the pattern number corresponding to each wavelength, as shown for several selected wavelengths in Fig. 2(a). The resulting quadratic relation between central wavelength and pattern number was used to calibrate the DMD. We note that this process had to be repeated each time the device was realigned, but only took ~ 1 min to do so.

An example of a calibrated spectrum is shown in Fig. 2(b), where the y axis represents the time difference Δt between pump and probe. The measured spectrum has a spectral resolution of 2.87 nm, defined as the average wavelength interval per pattern. The resolution can be improved by adjusting the spatial dispersion of the beam incident upon the DMD. We separately confirmed that a measurement of the visible portion of the spectrum produced by the fiber calibrated using this technique was consistent with that of a spectrometer. The data in Fig. 2(b) also demonstrate the stability of the spectrum over the entire 68-minute time window of the measurement. Since drift is recorded for both the reflectance R and its photoinduced change ΔR simultaneously, it is removed in the final processed data.

We chose a (110) oriented, N-type undoped Ge wafer sample (MTI Corporation - GEUe100505S1R50) due to its large pump–probe signal and excellent surface quality. Figure 3(a) shows the raw time-resolved change of reflectivity as a function of time and probe wavelength ΔR obtained by the demodulated difference frequency. The data were acquired using 300 raster scans (i.e., averages) of the spectrum. We observe that there is a large change in signal amplitude at $t = 0$ due to photoexcitation by the pump, while time $t = 0$ varied as a function of wavelength due to the uncompensated dispersion in the probe arm of the setup. Since the CM in Fig. 1 only compensates for the dispersion before the fiber, we separately corrected for chirp in the broadband probe obtained during supercontinuum generation and from the collimating objective in software. This was done by acquiring a time versus wavelength trace and modeling the dispersion by a quadratic

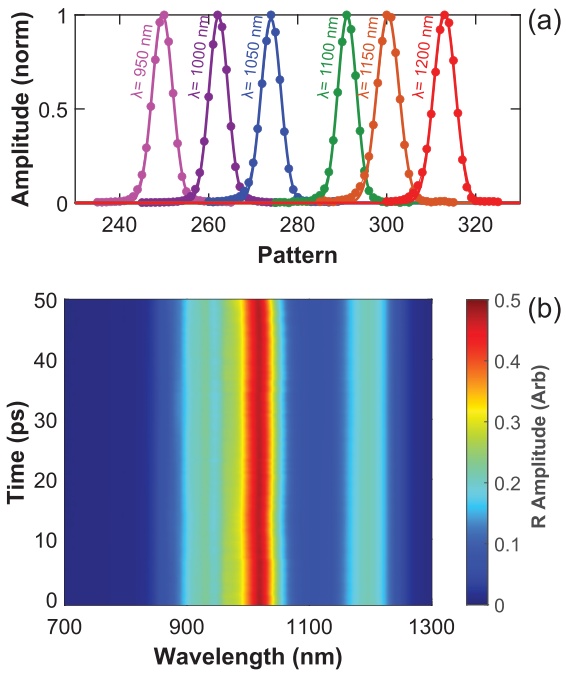

Fig. 2. (a) DMD calibration in the 950–1200-nm wavelength range. Data points for different choices of bandpass filter are shown as filled circles while Gaussian fits for the different data traces are shown as solid lines, allowing correspondence between pattern number and wavelength. The fits yielded an average 2.6 nm/pattern resolution. (b) Measured supercontinuum spectrum as reflected from a germanium test sample. The spectrum shows excellent stability over the 68-min data acquisition window.

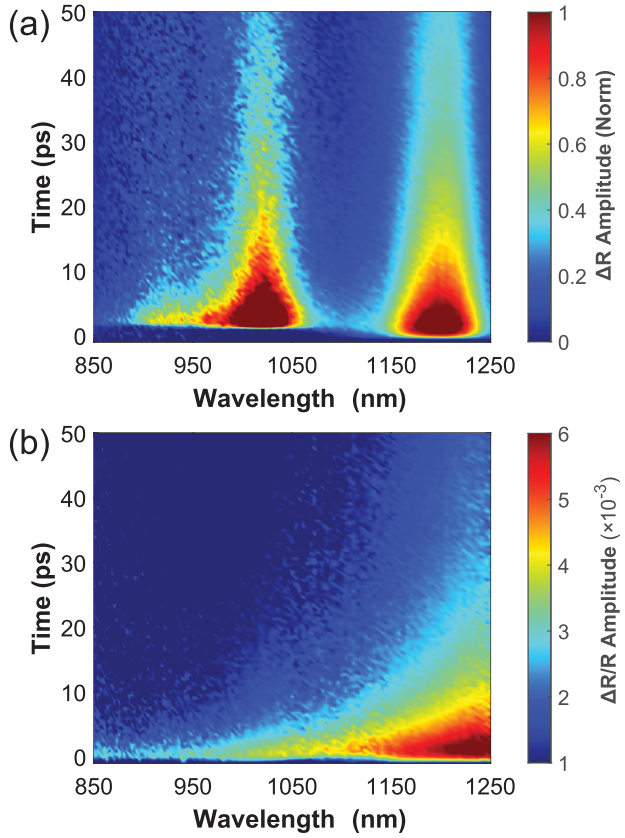

Fig. 3. Time-resolved optical pump, supercontinuum probe from Ge wafer sample. (a) Raw time and spectrally resolved ΔR as a function of incident wavelength and probe delay. (b) Normalized $\Delta R/R$ data produced by dividing the data from panel (a) by the data from Fig. 2(b)

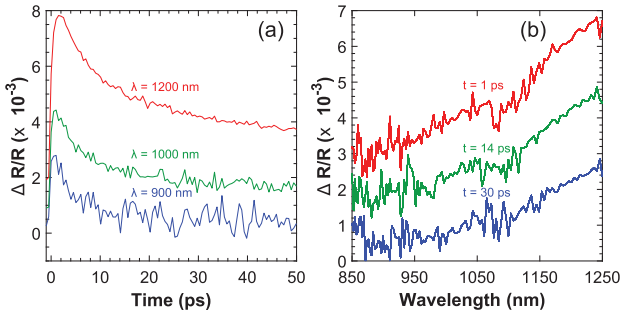

Fig. 4. Cuts along (a) wavelength and (b) time axes of the processed data. Each subsequent data trace is offset for clarity for both sets of plots.

function to obtain a correction equation to shift the time points during data analysis; a suitably chosen chirped mirror pair for the probe supercontinuum spectrum could obviate this step.

Although not visible in Fig. 3(a), we also observed a measurable response before time $t = 0$ in the ΔR channel. We attribute this artifact to the rapidly changing probe amplitude as the dispersed beam is raster-scanned by the DMD into the photodiode, which creates measurable signals at the demodulated frequencies. We verified that this artifact may be easily removed by simply averaging data points before $t = 0$ to generate a wavelength-dependent vector that is then subtracted from the entire ΔR matrix.

A post-processed version of the data from Figs. 2(b) and 3(a) are shown in Fig. 3(b). We observe the photoexcitation at time $t = 0$ as a sharp increase in the signal amplitude followed by a decay back to equilibrium at later time. As the probe photon wavelength increases, the photoexcited carrier decay time is also observed to increase, reflecting the changing carrier relaxation dynamics approaching the Ge bandgap.

Figure 4(a) displays cuts of the data in Fig. 3(b) along the time axis taken at wavelengths $\lambda = 900$, 1000, and 1200 nm. We observe good signal to noise for data taken within the wavelength range that the fiber produces strong output, while a noisier response was recorded for wavelengths at which the probe spectrum is weaker, suggesting the probe amplitude as the limiting variable in the signal to noise. We also determined that the temporal resolution was $\lesssim 400$ fs (see Supplement 1 for more details); however, significantly better temporal resolution can be achieved if the collimating objective after the fiber is replaced by a reflective optic and/or the supercontinuum spectrum is recompressed with a suitable chirped mirror pair or other recompression scheme [25,26].

Also shown in Fig. 4(b) are cuts along the energy axis at 1, 14, and 20 ps following the arrival of the pump beam which show the transfer of spectral weight as a function of delay time of the probe. Again, it can be seen in the figure that the less noisy data appear in the wavelength intervals where the fiber produces its brightest output, showing that detector responsivity did not seem to affect data quality as much as probe power incident

upon the detector. This is due to light loss from both the sample and from the DMD; of the 2.6 mW of power that reached the prism, only ~ 0.6 mW of the entire probe power was collected in reflection from the DMD. Since each pattern consists of a small subset of the entire beam, using less light in the fiber may require more sensitive detection equipment than the simple amplified photodiode used here.

We remark that the signal-to-noise ratio (SNR) of Fig. 4 is lower than can be obtained with visible spectrum supercontinuum-based pump–probe methods based on a typical camera and spectrometer, as well as other spectral fast scanning amplifier-based techniques [27], which can all generally measure reflectivity changes of the order of 10^{-5} with carefully designed apparatus [28]. The SNR here is also relatively low for an oscillator-based experiment, instead being more on par with lower repetition-rate, amplifier-based systems, as can be seen from the data in Fig. S4 of Supplement 1. Another contributing factor beyond low light levels were the small number of averages per time step (i.e., 300) used here, necessitated by the serialized nature of data acquisition. Most importantly, however, the use of an amplified, uncooled, large active area InGaAs detector was a significant source of noise. Measurements using similar experimental parameters but instead using a small active area, amplified silicon detector yielded significantly higher SNR noise of the level of $\pm 2 \times 10^{-5}$, as can be seen in Fig. S5 of Supplement 1. We thus suggest that using a small active area, cooled InGaAs detector with more averaging will significantly improve the quality of the data produced by this apparatus.

It is important to compare the advantages and disadvantages of this approach with more standard supercontinuum probe techniques. The traditional detection scheme comprising a spectrometer and a camera is easier to align than this setup, provides good SNR, and can operate faster than this apparatus due to the parallelized detection afforded by the camera. However, there are numerous advantages to the apparatus presented here. From a financial point of view, being able to conduct supercontinuum probing without the need for an amplified system presents a huge cost saving, while changing wavelength bands requires a new fiber and single-element detector, which may be cheaper than a new grating and camera. The optical layout presented here allows for quick and easy changes to spectral resolution and center wavelength while replacing and adjusting only a few low-cost optics, as opposed to spectrometer-based designs that would require swapping out gratings. This approach also does not need a low ambient light environment unless a photomultiplier tube is used as the single-element detector.

Simultaneous fast scanning of both time [29] and spectral axes at incommensurate frequencies could be implemented to sample every time and wavelength point in a quasi-random order, removing the effects of long-term drift from the data. Finally, we note that more sophisticated single-pixel imaging techniques implementing orthonormal bases such as the Hadamard basis, or the use of compressive sensing can further enhance the signal-to-noise ratio by increasing the amount of measured probe light per pattern while potentially speeding up data acquisition to the point that it could be competitive with parallelized detection.

In conclusion, we have described the design of a time-resolved optical pump, supercontinuum probe spectrometer based on a nonlinear photonic crystal fiber and single-pixel imaging with a spectral resolution of 2.6 nm and pre-recompressed temporal resolution $\lesssim 400$ fs. Currently, our technique is limited to the normal dispersion wavelength band of the supercontinuum generating fiber, i.e., 750–1250 nm for the FemtoWhite 800. Choosing fibers with different normal-dispersion regimes along with an appropriate single-element detector will permit this technique to be applied to the measurements in other wavelength ranges.

Funding. National Science Foundation (NSF/DMR-1945222).

Acknowledgments. We acknowledge Emre Ergeçen for useful discussions.

Disclosures. The authors declare no conflicts of interest.

Data availability. Data presented in this paper may be obtained from the authors upon reasonable request.

Supplemental document. See Supplement 1 for supporting content.

REFERENCES

1. Y.-X. Yan and K. A. Nelson, J. Chem. Phys. **87**, 6240 (1987).
2. L. Dhar, J. A. Rogers, and K. A. Nelson, Chem. Rev. **94**, 157 (1994).
3. A. Othonos, J. Appl. Phys. **83**, 1789 (1998).
4. F. Rossi and T. Kuhn, Rev. Mod. Phys. **74**, 895 (2002).
5. P. M. Norris, A. P. Caffrey, R. J. Stevens, J. M. Klopf, J. T. McLeskey, and A. N. Smith, Rev. Sci. Instrum. **74**, 400 (2003).
6. P. Kukura, D. W. McCamant, and R. A. Mathies, Annu. Rev. Phys. Chem. **58**, 461 (2007).
7. D. Polli, M. Rini, S. Wall, R. Schoenlein, Y. Tomioka, Y. Tokura, G. Cerullo, and A. Cavalleri, Nat. Mater. **6**, 643 (2007).
8. M. Fushitani, Annu. Rep. Prog. Chem., Sect. C: Phys. Chem. **104**, 272 (2008).
9. V. Gridnev, Phys. Rev. B **77**, 094426 (2008).
10. R. Berera, R. van Grondelle, and J. Kennis, Photosynth. Res. **101**, 105 (2009).
11. M. C. Fischer, J. W. Wilson, F. E. Robles, and W. S. Warren, Rev. Sci. Instrum. **87**, 031101 (2016).
12. D. R. Dietze and R. A. Mathies, ChemPhysChem **17**, 1224 (2016).
13. R. C. Prince, R. R. Frontiera, and E. O. Potma, Chem. Rev. **117**, 5070 (2017).
14. R. Geneaux, H. J. Marroux, A. Guggenmos, D. M. Neumark, and S. R. Leone, Phil. Trans. R. Soc. A. **377**, 20170463 (2019).
15. S. A. Kovalenko, A. L. Dobryakov, J. Ruthmann, and N. P. Ernsting, Phys. Rev. A **59**, 2369 (1999).
16. P. J. M. Johnson, V. I. Prokhorenko, and R. J. D. Miller, Opt. Express **17**, 21488 (2009).
17. L. De Boni, C. Toro, and F. E. Hernández, Opt. Express **16**, 957 (2008).
18. R. R. Alfano and S. L. Shapiro, Phys. Rev. Lett. **24**, 584 (1970).
19. B. Zhou and M. Bache, APL Photonics **1**, 050802 (2016).
20. M. F. Duarte, M. A. Davenport, D. Takhar, J. N. Laska, T. Sun, K. F. Kelly, and R. G. Baraniuk, IEEE Signal Process. Mag. **25**, 83 (2008).
21. M. P. Edgar, G. M. Gibson, and M. J. Padgett, Nat. Photonics **13**, 13 (2019).
22. J. M. Dudley, G. Genty, and S. Coen, Rev. Mod. Phys. **78**, 1135 (2006).
23. K. M. Hilligsøe, T. V. Andersen, H. N. Paulsen, C. K. Nielsen, K. Mølmer, S. Keiding, R. Kristiansen, K. P. Hansen, and J. J. Larsen, Opt. Express **12**, 1045 (2004).
24. N. M. Kearns, A. C. Jones, M. B. Kunz, R. T. Allen, J. T. Flach, and M. T. Zanni, J. Phys. Chem. A **123**, 3046 (2019).
25. D. Polli, D. Brida, S. Mukamel, G. Lanzani, and G. Cerullo, Phys. Rev. A **82**, 053809 (2010).
26. A. M. Heidt, J. Rothhardt, A. Hartung, H. Bartelt, E. G. Rohwer, J. Limpert, and A. Tünnermann, Opt. Express **19**, 13873 (2011).
27. G. Auböck, C. Consani, R. Monni, A. Cannizzo, F. Van Mourik, and M. Chergui, Rev. Sci. Instrum. **83**, 093105 (2012).
28. A. L. Dobryakov, S. A. Kovalenko, A. Weigel, J. L. Pérez-Lustres, J. Lange, A. Müller, and N. P. Ernsting, Rev. Sci. Instrum. **81**, 113106 (2010).
29. D. Edelstein, R. Romney, and M. Scheuermann, Rev. Sci. Instrum. **62**, 579 (1991).